Research Article

Yoshito Y. Tanaka*, Tomoya Kimura and Tsutomu Shimura

Unidirectional emission of phase-controlled second harmonic generation from a plasmonic nanoantenna

https://doi.org/10.1515/nanoph-2021-0470
Received August 21, 2021; accepted September 29, 2021;
published online October 13, 2021

Abstract: Shaping the emission pattern of second harmonic (SH) generation from plasmonic nanoparticles is important for practical applications in nonlinear nanophotonics but is rendered challenging by the complex second-order nonlinear-optical processes. Here, we theoretically and experimentally demonstrate that a pair of V- and Y-shaped gold nanoparticles directs the SH emission perpendicularly to an incident light direction. Owing to spatial overlap of two orthogonal plasmonic dipole modes at the fundamental and SH wavelengths of the individual particles, surface SH polarizations induced by the fundamental field is efficiently near-field coupled to the SH plasmon mode, resulting in dipolar SH emission from the individual particles. Moreover, the phase of this emission can be tuned simply by altering the part of the Y-particle shape, which changes the SH plasmon resonance while keeping the fundamental resonance. Our approach is a promising platform for engineering not only directional nonlinear nanoantennas but also nonlinear metamaterials.

Keywords: nonlinear plasmonics; phase control; plasmonic nanostructures; second harmonic generation; unidirectional emission.

1 Introduction

Controlling the nonlinear optical processes in nanoparticles is critical for practical applications in imaging [1–4], label-free sensing [5], and the selective identification [6, 7] of biomaterials. To obtain sufficient signals from nanoscale nonlinear light sources, which are inherently weak, many efforts have been devoted to increasing the nonlinear conversion efficiency. Especially, metal nanoparticles, supporting localized surface plasmon resonances, have been extensively studied because the plasmon-enhanced electromagnetic field can increase the conversion efficiency [8–18]. However, uncontrollable geometric defects, such as surface roughness and misalignments of the realistic metal particles, dramatically modify the emission patterns of second harmonic (SH) generation even without affecting the linear response [19–22]. Such disruptions to the SH emission reduce the collection efficiency and reproducibility in the measurements.

Although second-order nonlinear-optical effects are forbidden in centrosymmetric materials such as metals within the electric-dipole approximation [23], a SH polarization that radiates the electromagnetic field with doubled frequency of the incident light is generated at the metal surface where this symmetry is locally broken. As SH polarizations are primarily induced by the component of the electric field normal to the surface at the fundamental wavelength [24, 25], the surface shape and roughness directly affect the orientation of the SH polarizations. This wayward orientations of the SH polarizations are a common cause of uncontrollable SH emission patterns from metal nanoparticles.

The localized plasmon resonances of nanoantennas can be engineered to shape the emission patterns of nanoscale light emitters. In particular, multi element dipole antennas with carefully designed phase differences enable unidirectional light emission [26–29]. For instance, omnidirectional dipole-like emission from emitters such as quantum dots and organic dye molecules has been collimated into one direction by near-field coupling of the emitters to dipole antennas, thereby improving the efficiency of collection. Some theoretical studies [30, 31] have shown that SH emission from a metal nanosphere with no plasmon resonance at the SH wavelength can be directionally controlled by applying other passive structures, such as dielectric nanoparticles or a large nanocup cavity as the reflector and

*Corresponding author: Yoshito Y. Tanaka, Institute of Industrial Science, The University of Tokyo, 4-6-1 Komaba, Meguro-ku, Tokyo 153-8505, Japan, E-mail: yoshito@iis.u-tokyo.ac.jp
Tomoya Kimura and Tsutomu Shimura, Institute of Industrial Science, The University of Tokyo, 4-6-1 Komaba, Meguro-ku, Tokyo 153-8505, Japan

Open Access. © 2021 Yoshito Y. Tanaka et al., published by De Gruyter. This work is licensed under the Creative Commons Attribution 4.0 International License.

director. However, the experimental realization of these techniques is difficult because realistic metal particles are inherently rough-surfaced. Moreover, the precise phase control of SH emission from individual metal particles has been rendered challenging by complex second-order nonlinear-optical processes [14, 22, 32].

Here, we demonstrate unidirectional SH emission of a plasmonic nanoantenna via phase-controlled coupling of the surface SH polarizations to the plasmonic dipole modes of individual antenna elements at the SH wavelength. Spatial overlap of two orthogonal plasmonic dipole modes at the fundamental and SH wavelengths in a single element allows the efficient near-field coupling of the SH polarization induced by the fundamental field to the SH plasmon mode. The emission phase is precisely controlled by changing the plasmon resonance at the SH wavelength while keeping the resonance at the fundamental wavelength. After careful design of the phase difference and distance between the two elements composing the antenna, directional SH emission is achieved as illustrated in Figure 1A.

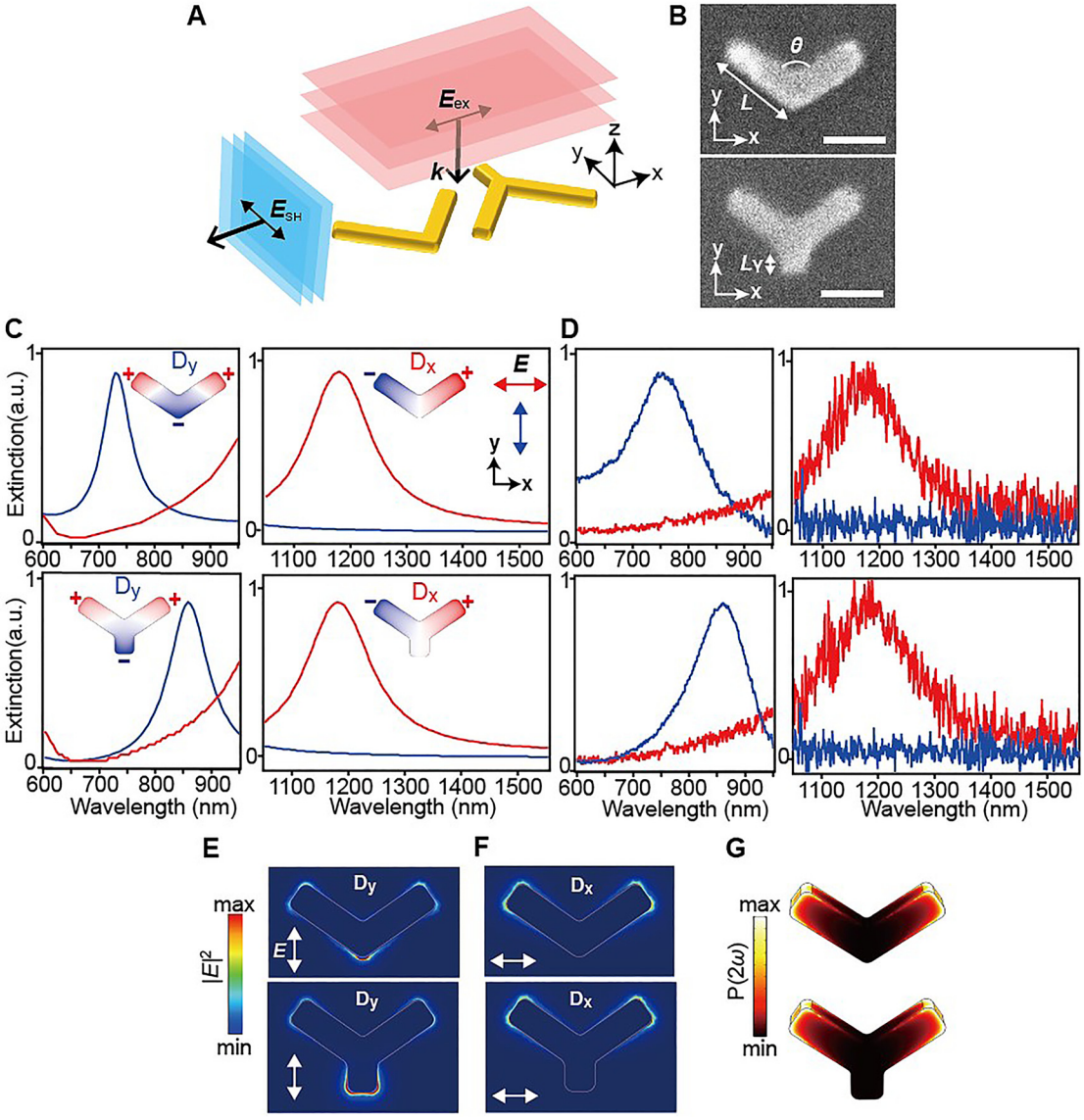

Figure 1: Characteristics of V- and Y-shaped elements in a directional second-harmonic (SH) gold nanoantenna.
(A) Unidirectional SH emission from a nanoantenna. (B) SEM images of the V- and Y-elements with arm length L = 140 nm, opening angle θ = 110°, and tail length L_Y = 30 nm (L_Y = 0 for the V-element). The scale bar is 100 nm. (C and D) Calculated and measured extinction spectra, respectively, of the individual elements in (B) under x-(red) and y-(blue) polarized illuminations. The insets show the phase distributions D_x and D_y of the plasmon modes oriented along the x- and y-polarizations, respectively. The D_x bands of the both elements are almost identical, but the D_y resonance wavelength is longer in the Y-element than in the V-element. (E and F) Calculated near-field intensity distributions of the D_y and D_x modes, respectively, of the V- and Y-elements. (G) Calculated spatial distributions of the surface SH polarization induced by the D_x near-fields in (F).

2 Results and discussion

2.1 Characteristics of nanoantena elements

From the selection rules for SH generation of isolated single metal nanoparticles, which are derived from parity conservation laws [33, 34], the general SH-emission patterns are based on quadrupoles and clearly differ from the dipolar scattering pattern in linear response [19, 22, 35, 36]. Meanwhile, the near-fields of multiple elements with different dipole resonances at their fundamental and SH wavelengths can spatially overlap at the fundamental and SH wavelengths, allowing dipolar SH emission [13, 14, 16, 37]. To obtain a compact and simple configuration, we overlap the spatial modes within a single element featuring two orthogonal plasmonic dipole modes. Figure 1B shows scanning electron microscope (SEM) images of the V- and Y-shaped nanoparticles studied in this work. These particles were fabricated on a glass coverslip by electron-beam lithography combined with a lift-off process. They were composed of evaporated gold with a thickness of 30 nm. Their geometries are defined by their arm length L, opening angle of the arms θ, and tail length L_Y (L_Y = 0 for the V-particle). The extinction spectra of both particle shapes exhibit two main resonance bands at visible and near-infrared wavelengths under *y*- and *x*-polarized illuminations, respectively (see Figure 1C and D). Their corresponding phase distributions (insets of Figure 1C and D) show orthogonal plasmonic dipole modes D_x and D_y along the incident *x*- and *y*-polarizations, respectively. The D_x band of the V-particle almost coincides with that of the Y-particle because it is determined by the length and opening angle of the arms (i.e., L and θ, respectively). Increasing the tail length L_Y shifts the D_y resonance wavelength to the red side (see also Figure S1) [38]. The near-field intensity distribution of the D_x mode overlaps with that of D_y at the end of each arm (Figure 1E and F). Moreover, the SH polarization in Figure 1G, induced by the D_x near field, should allow phase matching with the D_y mode. These results indicate that the SH polarization can be coupled to the D_y mode, where D_x and D_y are associated with active and passive modes, respectively.

2.2 Dipolar SH emission from a single element

To demonstrate this near-field coupling, we analyzed the angular distributions of SH-emission intensity from the V-shaped nanoparticle (Figure 2). The SH wavelength was matched to the D_y resonance peak at 750 nm in Figure 1C. Although the excitation (fundamental) wavelength at 1500 nm was far from the D_x resonance peak, the D_x mode was excited as confirmed in the near-field and charge distributions (see Figure S2). The magnitude of the SH emission is typically proportional to both of not only the square of the near-field of the fundamental mode, i.e., the D_x field in this study, but also the mode field at the SH wavelength, i.e., the D_y field [39]. Indeed, a strong enhancement of the SH emission for the V-shaped nanoparticle under the similar excitation condition has been demonstrated, even though the fundamental-mode field is not resonantly enhanced [40]. The distributions of azimuthal angle φ and polar angle θ in Figure 2A were measured using back focal plane (BFP) imaging [41]. When nanoparticles are placed on the high-refractive-index substrate, the maximum radiation to the substrate is observed at angles equal to or greater than the critical angle of the substrate interface [42]. Under *x*-polarized illumination, the V-particle exhibited *y*-polarized dipole-like SH emission which were maximized near the critical angle of ~41.14° for an air-glass interface (Figure 2B and D). The SH emission pattern and its polarization distribution well agreed with those of light scattering in the linear response to *y*-polarized light at 750 nm, which directly excites the D_y mode (Figure 2C and E). This result shows that the induced SH polarization was efficiently coupled to the D_y mode orthogonal to the incident polarization. It should be noted that coupling via the spatial overlap and phase matching between orthogonal dipole modes circumvents the selection rule even for an isolated nanoparticle.

2.3 SHG phase control

Our directional SH nanoantenna requires precise phase control of the dipolar SH emissions from individual elements. The surface SH polarization at a certain position $\mathbf{r}$ can be written as $P_{\mathrm{nnn}}(\mathbf{r}, 2\omega) = \varepsilon_0 \chi^{(2)}{}_{\mathrm{nnn}} E_{\mathrm{n}}(\mathbf{r}, \omega) E_{\mathrm{n}}(\mathbf{r}, \omega)$, where $\chi^{(2)}{}_{\mathrm{nnn}}$ and $E_{\mathrm{n}}(\mathbf{r}, \omega)$ are the components of the surface susceptibility tensor and electric field, respectively, normal to the surface of the nanoparticle at the fundamental (excitation) wavelength (a detailed explanation is provided in Section S1). These components are known to dominate the surface SH response of metal nanoparticles [24, 25]. From the above equation, the phase of the SH polarization can be determined from the phase of $E_{\mathrm{n}}(\mathbf{r}, \omega)$. When the excitation wavelength is much longer than the resonant wavelength, both the electric near-field and plasmon of the dipole mode oscillates in-phase with the excitation. As the excitation wavelength approaches the resonance peak, their relative phases shift by π around the resonance spectral position (Figure S3). However, in our case, the SH

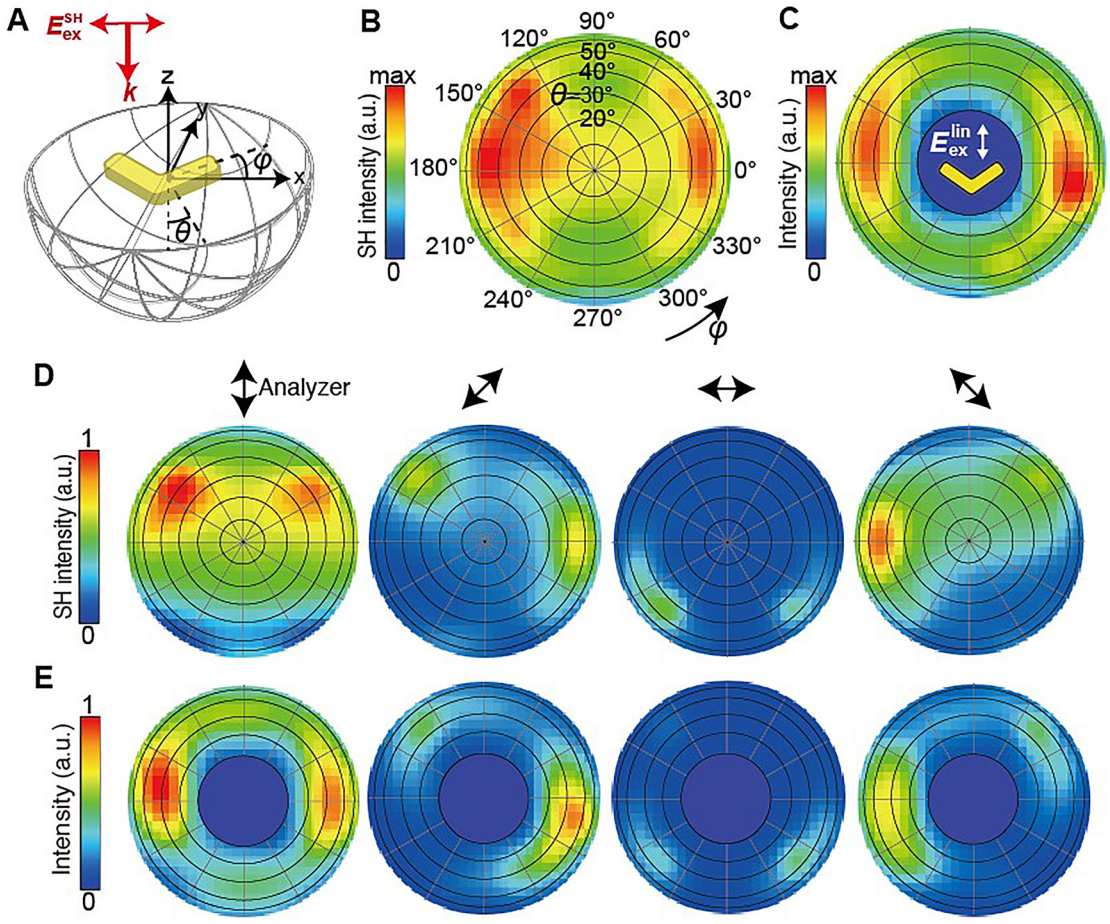

Figure 2: (A) Illustration of the coordinate system. The incident light is polarized along the *x*-direction to excite the D_x mode for the SH generation. (B) Measured angular distributions of the SH-emission intensity from the V-shaped element on the substrate in Figure 1. The azimuthal angle φ and polar angle θ in (A) were obtained using back focal plane imaging (41). The SH wavelength matches the D_y resonance peak at 750 nm. (C) Measured light scattering pattern in the linear response to *y*-polarized light illumination at 750 nm, which directly excites the D_y mode. (D and E) Polarization analysis of the SH-emission intensity in (B) and the linear scattering intensity in (C), respectively, obtained through an analyzer. The results are in good agreement with each other. The color scale indicates the normalized scattered light intensity.

wavelength must remain near the D_y resonance peak to obtain the stable dipolar SH emission (a detailed explanation is provided in Section S2). Because the excitation wavelength remains far from the D_x resonance peak, the phase control of the SH polarization is restricted. To control the phase of the dipolar SH emission, we instead focus for the first time on the phase shift in the coupling of the SH polarization to the D_y mode. The D_y resonance wavelength can be controlled through the tail length L_Y of the Y-shaped nanoparticle (Figure S1) without changing the D_x band, i.e., the phase of the induced SH polarization (see Figure 1). Under this control method, the effect of the D_y resonance on the phase of the SH emission can be simply analyzed.

The D_y resonance effect was revealed by observing the interference between the dipolar SH emissions from the V- and Y-shaped nanoparticles (Figure 3A). When two coherent dipoles with separation distance d oscillate with a phase difference $\Delta\Phi$, the retardation phase kd due to propagation of their radiation with wavenumber k can compensate $\Delta\Phi$ in one direction along the line connecting the dipoles, and add in the opposite direction. When two dipoles have equal magnitude, their radiation power is proportional to $\cos((\Delta\Phi + kd)/2)$ in one direction and $\cos((\Delta\Phi - kd)/2)$ in the other. In the present study, the SH wavelength λ_{SH} and distance d between the nanoparticles were fixed at 725 and 180 nm ($\sim\lambda_{SH}/4$), respectively, giving $k_{SH}d \sim \pi/2$ (Figure 3B and C). Therefore, depending on $\Delta\Phi$, the dipolar SH emissions constructively interfere in one direction along the *x*-axis and destructively interfere in the opposite direction. The pairs of V- and Y-nanoparticles were periodically arranged with a pitch of 650 nm in the *x*-direction to increase the signal-to-noise ratio of the SH

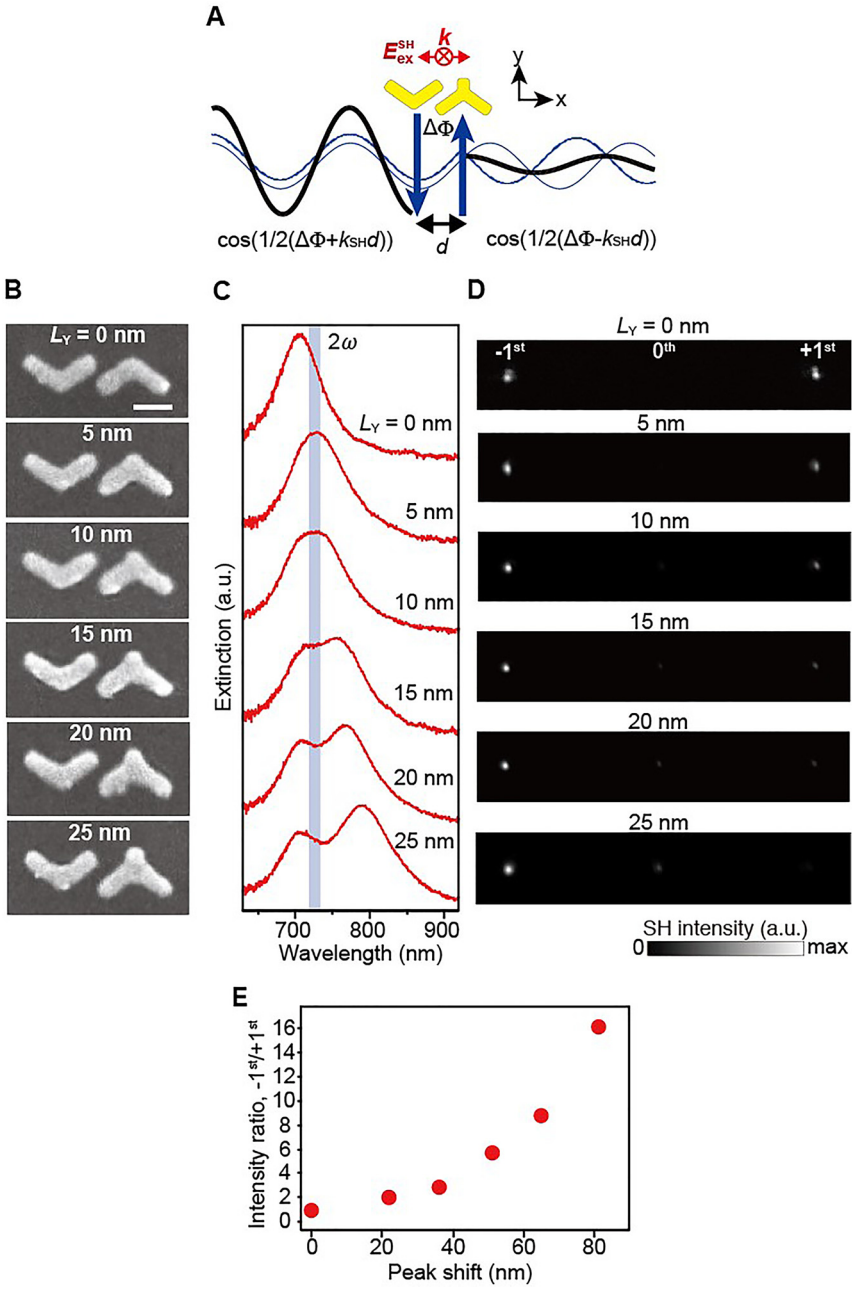

Figure 3: Phase control of the dipolar SH emission.
(A) Interference between two coherent dipoles separated by distance d, oscillating with phase difference ΔΦ. When the SH wavelength λ_{SH} and d are fixed, the ΔΦ between the dipolar SH emissions from the V- and Y-elements causes constructive and destructive interferences in opposite directions along the x-axis. (B, C, and D) SEM images, extinction spectra of D_y modes and measured diffraction patterns of SH emissions, respectively, of pairs of V- and Y-elements (L = 120 nm and θ = 110°) with different tail lengths L_Y. The scale bar in (B) is 100 nm. λ_{SH} and d are 725 nm (blue stripe in (C)) and 180 nm (~$\lambda_{SH}/4$), respectively, giving $k_{SH}d \sim \pi/2$. In (D), the individual pairs are arranged in a two-dimensional array (Λ_x = 650 nm and Λ_y = 800 nm) to increase the signal-to-noise ratio of the SH interference signals along the x-axis due to the diffraction grating effect. (E) Correlation between the SH intensity ratio of the ±1st diffraction orders [labeled −1st and +1st in (D)] and the peak shift of the D_y resonance of the Y-element in (C).

interference signals due to the diffraction grating effect [43]. In this configuration, the ΔΦ-dependent interference can be seen as light diffraction in the +1st and −1st orders along the x-axis. The intensity ratio of the ±1st order diffracted SH emissions as well as the D_y resonance clearly depended on the tail length L_Y of the Y-particle (see Figure 3C and D). When a pair of V-particles was used, i.e., L_Y = 0, the SH-emission pattern should be symmetric, with the same SH intensity of the +1st and −1st diffraction orders. In addition, ΔΦ should be π because the intensity of the 0th order diffracted SH emission was attenuated by destructive interference. As the D_y resonance redshifts with increasing L_Y, the SH intensity ratio in the ±1st diffraction orders increased in Figure 3(D and E), meaning that ΔΦ approaches $3\pi/2$ of the optimal conditions of radiation asymmetry. As the D_x band that determines the phase of the SH polarization is independent of L_Y (Figure S4), the asymmetry of the ±1st diffraction orders arises from the redshifted D_y resonance of the Y-particle at the SH wavelength. In other words, the phase of the dipolar SH emission can be controlled simply by changing L_Y (which alters the D_y resonance). By this method, we can precisely design the SH phase differences between the elements in the nanoantenna. Moreover, these results strongly support

that the SH signal was emitted by the induced SH polarization coupled to the D_y mode rather than directly from the SH polarization.

2.4 Directional SH emission from a nanoantenna

To further understand the behavior of the directional SH nanoantenna, we measured the wavelength dependence of the SH-emission patterns from a single pair of V- and Y-shaped nanoparticles with a tail length of 25 nm for the Y-particle (see Figure 3B). The maximum directivity of the SH emission, i.e., perfect constrictive and destructive interference in Figure 3A, can be achieved for $k_{SH}d \sim \pi/2 + m\pi$ ($m = 0, \pm1, \pm2\ldots$) and $\Delta\Phi = \pi/2 + n\pi$ ($n = 0, \pm1, \pm2\ldots$). The distance d between the nanoparticles was set to obtain the maximum directivity for the SH wavelength $\lambda_{SH} = 725$ nm, i.e., $k_{SH}d \sim \pi/2$. The phase difference $\Delta\Phi$ can be also optimized by controlling the excitation wavelength because $\Delta\Phi$ depends on the SH wavelength around the D_y resonance. Figure 4A displays the BFP images under x-polarized illumination at different wavelengths. The antenna exhibited strong lateral directionality at the SH

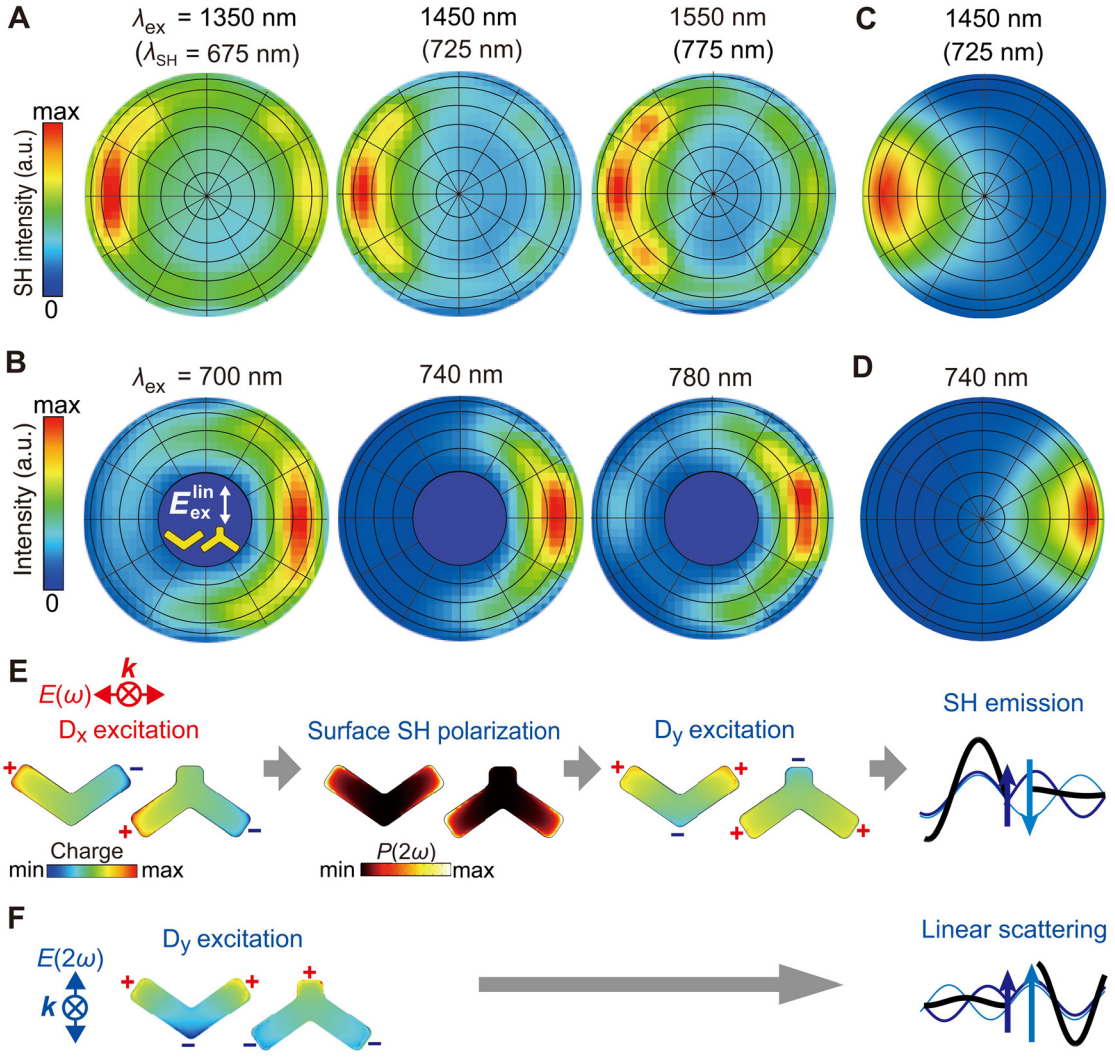

Figure 4: (A and B) Measured angular distributions of SH emission and linearly scattered light, respectively, from a pair of V- and Y-elements with a tail length of 25 nm (see Figure 3B) at different wavelengths of incident light. λ_{ex} and λ_{SH} denote the excitation and SH wavelengths, respectively. In (B), the D_y mode of the antenna was directly excited by y-polarized light illumination. The antenna directivities of both radiations were maximized in the wavelength range between the D_y resonances of the V- and Y-elements. The SH emission in (A) and linear scattering in (B) occurred in opposite directions. (C and D) Corresponding theoretical angular distributions of the SH emission at $\lambda_{ex} = 1450$ nm and the linearly scattered light at $\lambda_{ex} = 740$ nm, respectively. (E and F) Charge and SH polarization distributions in the processes leading to unidirectional radiation of (C) and (D), respectively.

wavelength λ_{SH} between the D_y resonance peaks of the V- and Y-elements. The intensity was maximized near the (φ, θ) = (180°, 45°) direction exceeding the critical angle. In general, nanoparticles emit light into a substrate with higher refractive index, and index-matching shifts the emission direction to θ = 90°. It should be noted that linear scattering at the fundamental wavelength λ_{ex} is omnidirectional, i.e., dipole radiation (Figure S5). In other words, the omnidirectional excitation of the antenna permits directional SH emission. To realize directional SH emission, we exploited the different plasmon modes of antenna excitation and SH emission. When the D_y modes of the antenna were directly excited by *y*-polarized light, the linear response was also unidirectional side scattering, similarly to that of SH emission (Figure 4B). Interestingly, the linear scattering and SH emission appeared in opposite directions, although the radiation patterns from the individual antenna elements were almost identical (Figure 2). These results are supported by numerical simulations (see Figure 4C and D). In the SH generation process, the D_y modes were excited by the SH polarization normal to the surface localized at the arm ends of the V- and Y-nanoparticles (Figure 1G). Therefore, the phase of the SH emission was flipped by inverting the Y-element in the antenna, as shown in Figure 4E. This explains the phase difference $\Delta\Phi = \pi$ between the SH emissions of a V-particle pair in Figure 3. Conversely, in the linear process, the incident *y*-polarized light excited the D_y modes of the V- and Y-elements in the antenna in-phase (Figure 4F). Thus, $\Delta\Phi$ of the SH emission from the directional antenna differed by π from that of linear light scattering, resulting in opposite propagation directions of the two emissions.

3 Conclusions

We experimentally demonstrated that a pair of V- and Y-shaped gold nanoparticles enables unidirectional SH emission perpendicularly to the incident light direction. Dipolar SH emission from the individual particles occurs through efficient near-field coupling of the surface SH polarization with the plasmonic dipole mode at the SH wavelength, which is orthogonal to the incident polarization. Moreover, the phase of the SH emission is precisely controlled simply by changing the tail length of the Y-particle, which alters the SH resonance. Similarly to the linear process, we can precisely design the SH phase distributions of elements in nonlinear nanoantennas and metasurfaces. This phase control is easily implemented in nanoantennas with coupled elements that strongly resonate at both fundamental and SH wavelengths [13, 14, 37]. Our approach offers a promising platform for realizing nonlinear nanophotonic technologies over a wide application range, from label-free sensing [43] to optical nanomotor [44], beam shaping [45] and optical communications [46].

4 Materials and methods

4.1 Nanoantenna fabrication

Nanoantennas were fabricated on a glass substrate using simple electron-beam lithography (EBL) and lift-off techniques. After washing a glass substrate, a film of the positive resist (ZEP520a, Zeon Chemicals Co.) was formed by spin-coating to a thickness of 200 nm. The film was exposed to a given pattern using an EBL system with a high accelerating voltage (125 kV) and was then sequentially developed in developer solution (ZED-N50, Zeon Chemicals Co.) and a rinsing agent (ZMD-B, Zeon Chemicals Co.). A 30-nm gold layer was deposited by electron-beam evaporation. The resist pattern was subsequently removed from the substrate using a resist remover (ZDMAC, Zeon Chemicals Co.), forming nanoantennas on the glass substrate.

4.2 Experimental characterization

To characterize the nonlinear and linear optical responses of the nanoantennas, we recorded the angular distributions of their SH-emission and linear-light-scattering intensities, respectively, using the BFP imaging setup depicted in Figure S6. The antennas were periodically arranged with a pitch of 2 μm. Their nonlinear and linear responses were obtained under a femtosecond pulsed laser (generated by an optical parametric amplifier) and a continuous-wave Ti:sapphire laser, respectively, with tunable wavelength ranges of 1300–1600 and 700–1000 nm, respectively. The linear polarization of the laser beams was changed to the desired direction by a half-wave plate. These laser beams were weakly focused on the antennas by a 4× objective lens with a numerical aperture (NA) of 0.13. The SH emission and linear scattering in the forward direction were collected through another 60× oil-immersion objective lens (NA = 1.49). The SHG excitation and stray light were removed by a 1150-nm cutoff short-pass filter and a 650-nm cutoff long-pass filter. To block the transmitted light while measuring the linear scattering pattern, an opaque stopper with a diameter corresponding to NA < 0.3 was installed in a secondary BFP. The BFP images were projected on a sCMOS camera and processed by a previously described method [47]. The polarizations of the SH signal and scattered light were selected by an absorptive sheet polarizer. Linear spectroscopic characterizations of the antennas were carried out using white light in the same illumination system as the laser beams. The extinction spectra of the antennas were obtained as $(I_b(\lambda) - I_m(\lambda))/I_b(\lambda)$, where $I_m(\lambda)$ and $I_b(\lambda)$ are the spectra of the transmitted white light through the substrates with and without antennas, respectively. The polarization dependences of the extinction spectra were analyzed by placing an absorptive sheet polarizer in front of the illumination objective. The spectra were measured in the wavelength ranges 600–950 and 1050–1600 nm using silicon and InGaAs detectors, respectively.

4.3 Theoretical characterization

The linear and nonlinear responses of the nanoantennas were numerically simulated with a full three-dimensional Maxwell calculation based on a finite element method solver (COMSOL). The nanoantennas were placed on a substrate with a refractive index n of 1.52. The radius of curvature at the corners of the nanoparticle was 10 nm. The wavelength dispersion of the complex permittivity of gold was measured by Johnson and Christy [48]. The simulation method of the nonlinear response is detailed in Section S1 of the Supplementary materials. The spatial distributions of the surface SH polarizations were obtained from the square of the fundamental electric field normal to the surface. The SH electric field radiated from the nanoantennas was computed as the excitation source of the surface polarizations oscillating at the SH frequency. The angular distributions of the SH emission were calculated from the pointing vectors on a 2-μm-diameter sphere surrounding the structure.

Author contributions: YYT and TK contributed equally. All the authors have accepted responsibility for the entire content of this submitted manuscript and approved submission.
Research funding: This work was supported by JSPS KAKENHI Grants No. JP19H02533, and No. JP19H04670 in Scientific Research on Innovative Areas "Nano-Material Optical-Manipulation".
Conflict of interest statement: The authors declare no conflicts of interest regarding this article.

References

[1] B. E. Cohen, "Biological imaging: beyond fluorescence," *Nature*, vol. 467, pp. 407–408, 2010.
[2] P. Pantazis, J. Maloney, D. Wu, and S. E. Fraser, "Second harmonic generating (SHG) nanoprobes for in vivo imaging," *Proc. Natl. Acad. Sci. USA*, vol. 107, pp. 14535–14540, 2010.
[3] G. Malkinson, P. Mahou, É. Chaudan, et al., "Fast in vivo imaging of SHG nanoprobes with multiphoton light-sheet microscopy," *ACS Photonics*, vol. 7, pp. 1036–1049, 2020.
[4] P. Mahou, G. Malkinson, É. Chaudan, T. Gacoin, E. Beaurepaire, and W. Supatto, "Metrology of multiphoton microscopes using second harmonic generation nanoprobes," *Small*, vol. 13, pp. 1–11, 2017.
[5] J. Butet, I. Russier-Antoine, C. Jonin, N. Lascoux, E. Benichou, and P.-F. Brevet, "Sensing with multipolar second harmonic generation from spherical metallic nanoparticles," *Nano Lett.*, vol. 12, pp. 1697–1701, 2012.
[6] K. Singh, D. Senapati, S. Wang, et al., "Gold nanorod based selective identification of *Escherichia coli* bacteria using two-photon Rayleigh scattering spectroscopy," *ACS Nano*, vol. 3, pp. 1906–1912, 2009.
[7] A. Neely, C. Perry, B. Varisli, et al., "Ultrasensitive and highly selective detection of Alzheimer's disease biomarker using two-photon Rayleigh scattering properties of gold nanoparticle," *ACS Nano*, vol. 3, pp. 2834–2840, 2009.
[8] K. Thyagarajan, J. Butet, and O. J. F. Martin, "Augmenting second harmonic generation using Fano resonances in plasmonic systems," *Nano Lett.*, vol. 13, pp. 1847–1851, 2013.
[9] R. Czaplicki, J. Makitalo, R. Siikanen, et al., "Second-harmonic generation from metal nanoparticles: resonance enhancement versus particle geometry," *Nano Lett.*, vol. 15, pp. 530–534, 2015.
[10] H. Aouani, M. Navarro-Cia, M. Rahmani, et al., "Multiresonant broadband optical antennas as efficient tunable nanosources of second harmonic light," *Nano Lett.*, vol. 12, pp. 4997–5002, 2012.
[11] K. Thyagarajan, S. Rivier, A. Lovera, and O. J. F. Martin, "Enhanced second-harmonic generation from double resonant plasmonic antennae," *Opt. Express*, vol. 20, pp. 12860–12865, 2012.
[12] H. Harutyunyan, G. Volpe, R. Quidant, and L. Novotny, "Enhancing the nonlinear optical response using multifrequency gold-nanowire antennas," *Phys. Rev. Lett.*, vol. 108, p. 217403, 2012.
[13] M. Celebrano, X. Wu, M. Baselli, et al., "Mode matching in multiresonant plasmonic nanoantennas for enhanced second harmonic generation," *Nat. Nanotechnol.*, vol. 10, pp. 412–417, 2015.
[14] S. D. Gennaro, M. Rahmani, V. Giannini, et al., "The interplay of symmetry and scattering phase in second harmonic generation from gold nanoantennas," *Nano Lett.*, vol. 16, pp. 5278–5285, 2016.
[15] W. Y. Tsai, T. L. Chung, H. H. Hsiao, et al., "Second harmonic light manipulation with vertical split ring resonators," *Adv. Mater.*, vol. 31, p. e1806479, 2019.
[16] A. Noor, A. R. Damodaran, I.-H. Lee, S. A. Maier, S.-H. Oh, and C. Ciracì, "Mode-matching enhancement of second-harmonic generation with plasmonic nanopatch antennas," *ACS Photonics*, vol. 7, pp. 3333–3340, 2020.
[17] J. Lee, S. Yang, J. Lee, et al., "Extraordinary optical transmission and second harmonic generation in sub-10-nm plasmonic coaxial aperture," *Nanophotonics*, vol. 9, pp. 3295–3302, 2020.
[18] G. Li, D. Lei, M. Qiu, W. Jin, S. Lan, and A. V. Zayats, "Light-induced symmetry breaking for enhancing second-harmonic generation from an ultrathin plasmonic nanocavity," *Nat. Commun.*, vol. 12, p. 4326, 2021.
[19] J. Butet, K. Thyagarajan, and O. J. F. Martin, "Ultrasensitive optical shape characterization of gold nanoantennas using second harmonic generation," *Nano Lett.*, vol. 13, pp. 1787–1792, 2013.
[20] J. Butet and O. J. F. Martin, "Nonlinear plasmonic nanorulers," *ACS Nano*, vol. 8, pp. 4931–4939, 2014.
[21] G. Bautista, M. J. Huttunen, J. Mäkitalo, J. M. Kontio, J. Simonen, and M. Kauranen, "Second-harmonic generation imaging of metal nano-objects with cylindrical vector beams," *Nano Lett.*, vol. 12, pp. 3207–3212, 2012.
[22] J. Butet, T. V. Raziman, K. Y. Yang, G. D. Bernasconi, and O. J. Martin, "Controlling the nonlinear optical properties of plasmonic nanoparticles with the phase of their linear response," *Opt. Express*, vol. 24, pp. 17138–17148, 2016.
[23] R. W. Boyd, *Nonlinear Optics*, 3rd ed. Boston, Academic Press, 2008.
[24] F. X. Wang, F. J. Rodriguez, W. M. Albers, R. Ahorinta, J. E. Sipe, and M. Kauranen, "Surface and bulk contributions to the second-order nonlinear optical response of a gold film," *Phys. Rev. B*, vol. 80, p. 233402, 2009.
[25] G. Bachelier, J. Butet, I. Russier-Antoine, C. Jonin, E. Benichou, and P.-F. Brevet, "Origin of optical second-harmonic generation in spherical gold nanoparticles: local surface and nonlocal bulk contributions," *Phys. Rev. B*, vol. 82, p. 235403, 2010.

[26] G. Curto, G. Volpe, T. H. Taminiau, M. P. Kreuzer, R. Quidant, and N. F. van Hulst, "Unidirectional emission of a quantum dot coupled to a nanoantenna," *Science*, vol. 329, pp. 930–933, 2010.
[27] T. Kosako, Y. Kadoya, and H. F. Hofmann, "Directional control of light by a nano-optical Yagi–Uda antenna," *Nat. Photonics*, vol. 4, pp. 312–315, 2010.
[28] W. Zhu, D. Wang, and K. B. Crozier, "Direct observation of beamed Raman scattering," *Nano Lett.*, vol. 12, pp. 6235–6243, 2012.
[29] J. Ho, Y. H. Fu, Z. Dong, et al., ""Highly directive hybrid metal-dielectric Yagi–Uda nanoantennas," *ACS Nano*, vol. 12, pp. 8616–8624, 2018.
[30] X. Y. Z. Xiong, L. J. Jiang, W. E. I. Sha, Y. H. Lo, and W. C. Chew, "Compact nonlinear Yagi–Uda nanoantennas," *Sci. Rep.*, vol. 6, p. 18872, 2016.
[31] X. Y. Z. Xiong, L. J. Jiang, E. Wei, et al., "Strongly enhanced and directionally tunable second-harmonic radiation from a plasmonic particle-in-cavity nanoantenna," *Phys. Rev. A*, vol. 94, p. 053825, 2016.
[32] S. G. Rodrigo, H. Harutyunyan, and L. Novotny, "Coherent control of light scattering from nanostructured materials by second-harmonic generation," *Phys. Rev. Lett.*, vol. 110, p. 177405, 2013.
[33] M. Finazzi, P. Biagioni, M. Celebrano, and L. Duò, "Selection rules for second-harmonic generation in nanoparticles," *Phys. Rev. B*, vol. 76, p. 125414, 2007.
[34] J. Butet, S. Dutta-Gupta, and O. J. F. Martin, "Surface second-harmonic generation from coupled spherical plasmonic nanoparticles: eigenmode analysis and symmetry properties," *Phys. Rev. B*, vol. 89, p. 245449, 2014.
[35] J. Butet, P. F. Brevet, and O. J. Martin, "Optical second harmonic generation in plasmonic nanostructures: from fundamental principles to advanced applications," *ACS Nano*, vol. 9, pp. 10545–10562, 2015.
[36] D. Smirnova and Y. S. Kivshar, "Multipolar nonlinear nanophotonics," *Optica*, vol. 3, pp. 1241–1255, 2016.
[37] K. Y. Yang, J. Butet, C. Yan, G. D. Bernasconi, and O. J. F. Martin, "Enhancement mechanisms of the second harmonic generation from double resonant aluminum nanostructures," *ACS Photonics*, vol. 4, pp. 1522–1530, 2017.
[38] M. A. Kats, P. Genevet, G. Aoust, et al., "Giant birefringence in optical antenna arrays with widely tailorable optical anisotropy," *Proc. Natl. Acad. Sci. USA*, vol. 109, pp. 12364–12368, 2012.
[39] K. O'Brien, H. Suchowski, J. Rho, et al., "Predicting nonlinear properties of metamaterials from the linear response," *Nat. Mater.*, vol. 14, pp. 379–383, 2015.
[40] H. Linnenbank and S. Linden, "Second harmonic generation spectroscopy on second harmonic resonant plasmonic metamaterials," *Optica*, vol. 2, pp. 698–701, 2015.
[41] Y. Y. Tanaka and T. Shimura, "Tridirectional polarization routing of light by a single triangular plasmonic nanoparticle," *Nano Lett.*, vol. 17, pp. 3165–3170, 2017.
[42] T. Shegai, B. Brian, V. D. Miljković, and M. Käll, "Angular distribution of surface-enhanced Raman scattering from individual au nanoparticle aggregates," *ACS Nano*, vol. 5, pp. 2036–2041, 2011.
[43] B. Evlyukhin, S. I. Bozhevolnyi, A. Pors, et al., "Detuned electrical dipoles for plasmonic sensing," *Nano Lett.*, vol. 10, pp. 4571–4577, 2010.
[44] Y. Y. Tanaka, P. Albella, M. Rahmani, V. Giannini, S. A. Maier, and T. Shimura, "Plasmonic linear nanomotor using lateral optical forces," *Sci. Adv.*, vol. 6, p. eabc3726, 2020.
[45] J. Scheuer, "Metasurfaces-based holography and beam shaping: engineering the phase profile of light," *Nanophotonics*, vol. 6, pp. 137–152, 2017.
[46] R. Guo, M. Decker, F. Setzpfandt, et al., "High-bit rate ultra-compact light routing with mode-selective on-chip nanoantennas," *Sci. Adv.*, vol. 3, p. e1700007, 2017.
[47] D. Vercruysse, Y. Sonnefraud, N. Verellen, et al., "Unidirectional side scattering of light by a single-element nanoantenna," *Nano Lett.*, vol. 13, pp. 3843–3849, 2013.
[48] P. B. Johnson and R. W. Christy, "Optical constants of the noble metals," *Phys. Rev. B*, vol. 6, pp. 4370–4379, 1972.

Supplementary Material: The online version of this article offers supplementary material (https://doi.org/10.1515/nanoph-2021-0470).